NATIONAL ADVISORY COMMITTEE FOR AERONAUTICS

TECHNICAL NOTE

No. 1487

EFFECT OF ASPECT RATIO AND TAPER ON THE

PRESSURE DRAG AT SUPERSONIC SPEEDS OF

UNSWEPT WINGS AT ZERO LIFT

By Jack N. Nielsen

Ames Aeronautical Laboratory
Moffett Field, Calif.

Washington

November 1947

NATIONAL ADVISORY COMMITTEE FOR AERONAUTICS

TECHNICAL NOTE NO. 1487

EFFECT OF ASPECT RATIO AND TAPER ON THE

PRESSURE DRAG AT SUPERSONIC SPEEDS OF

UNSWEPT WINGS AT ZERO LIFT

By Jack N. Nielsen

SUMMARY

The linear theory for determining the pressure distribution at supersonic speeds on wings of symmetrical section at zero lift has been used to calculate the pressure drag coefficients at zero lift of the family of unswept, untwisted wings with the diamond profile. On the basis of the method of R. T. Jones, which was presented in NACA TN No. 1107, a general expression has been found for the drag coefficient at any supersonic Mach number, aspect ratio, and taper. The general expression, which is too unwieldy for use in analysis, has been used in the construction of nondimensional charts permitting a rapid estimation of the drag coefficient for a given wing at any Mach number. For wings of diamond or rectangular plan form the general expression reduces to simple formulas for the drag coefficients. The nondimensional charts indicate that, at very low aspect ratios, wings of diamond plan form have the least drag and that increasing the ratio of tip chord to root chord increases the drag markedly. However, at large aspect ratios rectangular wings have the least drag and decreasing the ratio of tip chord to root chord increases the drag slightly.

INTRODUCTION

Methods for determining the aerodynamic characteristics of various aircraft components at supersonic speeds have recently become the subject of widespread attention. Of particular interest are methods which permit determination of wing characteristics in three-dimensional flow. Substantial progress in the development of a theory for the three-dimensional supersonic wing has been made by linearizing the problem on the basis of small perturbation theory. This makes possible the use of the superposition principle and enables separation of the pressures acting on an uncambered wing into (1) a pressure distribution due to thickness which occurs at zero angle of attack plus (2) a pressure distribtuion due

to angle of attack which occurs on a flat plate of the wing plan form at the wing angle of attack. The pressure distribution due to thickness for thin symmetrical wings the surfaces of which are formed by planes can be determined by the method of R. T. Jones (reference 1). Essentially the method consists of orienting oblique line pressure sources and oblique line pressure sinks of different strengths in a manner to satisfy the boundary conditions and then adding their pressure fields. An equivalent method has been published by Puckett (reference 2).

The foregoing methods have been rather extensively applied to wings of triangular plan form, but as yet only limited study of the effects of changing plan form by varying aspect ratio, taper, and sweep has been carried out. (Reference 3 is such a study.) Accordingly in this report the method of Jones has been applied to determining the pressure drag coefficient at zero lift of a family of untwisted wings of diamond profile differing in aspect ratio and taper. For all wings the line of maximum thickness, that is, the mid—chord line, is unswept. Tapers from zero to unity have been considered for all aspect ratios.

SYMBOLS

A   aspect ratio

s   semispan, feet

c   root chord, feet

C_D wing pressure—drag coefficient

M   free—stream Mach number

p   local static pressure, pounds per square foot

p_0 free—stream static pressure, pounds per square foot

P   pressure coefficient $\left(\dfrac{p-p_0}{q_0} \right)$

q_0 free—stream dynamic pressure, pounds per square foot

S   wing area, square feet

t   maximum thickness of wing section at root chord, feet

$\dfrac{t}{c}$ wing thickness ratio, fraction of chord, approximately equal to tangent of semivertex angle of wing section measured in streamwise direction

Λ sweep angle of leading edge, radians

θ polar angle measured from downstream direction, radians

σ tan θ

τ tan Λ

R.P.   real part of a complex quantity

λ wing taper, ratio of tip chord to root chord

Subscripts

a   leading-edge sources

b   midchord-line sinks

c   trailing-edge sources

d   leading-edge image sinks

e   midchord-line image sources

ANALYSIS

Types of Wings

For the purpose of the analysis it has been convenient to subdivide the wings under consideration into eight types as shown in figure 1. From this figure it can be seen that certain relationships between aspect ratio and taper define boundaries which determine the wing type. Along boundary III the leading and trailing edges are coincident with their respective Mach lines. Above this boundary the leading and trailing edges are swept in front of the Mach lines emanating from their foremost points and are termed supersonic leading and trailing edges. Below this boundary the leading and trailing edges are swept behind their respective Mach lines and are termed subsonic leading and trailing edges. This figure may be used for any Mach number by using $A\sqrt{M^2-1}$, the effective aspect ratio, in place of the aspect ratio.

In wings of type 1, the Mach lines all intersect the trailing edges of the adjacent half wing. In wings of type 2, the Mach lines from the extremities of the leading edges intersect the trailing edges of the opposite half wing, and the Mach lines from the leading

vertex intersect the wing tips at a point between the midchord line and the trailing edge. The differences between wings of other types can easily be seen in figure 1.

Determination of Wing Pressure Field

The wing pressure field can be built up by superimposing a number of simple pressure fields which are basically of two types. These types of pressure fields are those given by Jones in reference 1 for a semi-infinite symmetrical wedge swept in front of or behind the Mach line from its apex.

For a semi-infinite symmetrical wedge with a supersonic leading edge (fig. 2(a)) the pressure field is conical and for $M^2 = 2$ is given by the following equation:

$$P = R.P. \frac{2\,t/c}{\pi\sqrt{1 - \tan^2 \Lambda}} \cos^{-1} \frac{\tan \Lambda - \tan \theta}{\left| 1 - \tan \Lambda \tan \theta \right|} \qquad (1)$$

Between the leading edge where $\theta + \Lambda = \frac{\pi}{2}$ and the Mach line where $\tan \theta = 1$ this equation reduces to

$$P = \frac{2\,t/c}{\sqrt{1 - \tan^2 \Lambda}}$$

which is the Ackeret equation, as given by reference 4, for the pressure coefficient based on the Mach number component perpendicular to the leading edge. The pressure falls from this value at the Mach line where $\tan \theta = 1$ to 0 at the Mach line where $\tan \theta = -1$.

For a semi-infinite symmetrical wedge with a subsonic leading edge (fig. 2(b)) the conical pressure field is given by the following equation:

$$P = R.P. \frac{2\,t/c}{\pi\sqrt{\tan^2 \Lambda - 1}} \cosh^{-1} \frac{\tan \Lambda - \tan \theta}{\left| 1 - \tan \Lambda \tan \theta \right|} \qquad (2)$$

The pressure coefficient rises from zero at the near Mach line where $\tan \theta = 1$ to infinity at the leading edge and falls again to zero at the far Mach line where $\tan \theta = -1$.

It is convenient to consider the foregoing solutions for wedges as sources or sinks depending on whether they produce positive or negative pressures. Thus when a flow is symmetrically diverged as by a wedge, the changes in pressure are positive and can be considered the result of a pressure source coincident with the leading edge of the wedge. When a flow is symmetrically converged, as when flowing over the maximum thickness position of a diamond profile wing, the changes in pressure are negative and can be considered the result of a pressure sink lying along the midchord line.

The pressure fields of the sources and sinks which shape the wing are added to give the wing pressure field. From the leading apex two sources are swept back along the leading edges to infinity producing wedge boundaries along their entire extent (fig. 3(a)). To confine these wedge boundaries to the finite length of the leading edges of the wing, two image sinks of equal and opposite magnitude are superimposed onto the portions of the sources lying off the wing (fig. 3(b)), thereby producing in part the effect of a tip. Two semi-infinite sinks are placed along the midchord line at right angles to the flow, and two image sources are superimposed on those portions of the sinks lying beyond the wing tips (fig. 3(c)). The two image sources combined with the two aforementioned image sinks fully represent the effect of the tips. To return the flow at the trailing edge to its original direction, two sources (fig. 3(d)) are started at the extremities of the trailing edges and are extended back along the trailing edges to infinity intersecting at the trailing apex. The images of the trailing-edge sources cannot have any contribution to the wing pressures and need not be considered.

Wing Drag Coefficient

The contribution to the wing pressure drag of the pressure field of each source and sink can be individually determined, and the sum of the individual pressure drags will then be the total drag. This may be expressed in coefficient form as

$$C_D = C_{D_a} + C_{D_b} + C_{D_c} + C_{D_d} + C_{D_e} \tag{3}$$

where the symbols have the following meanings:

C_{D_a} drag coefficient associated with the leading-edge sources

C_{D_b} drag coefficient associated with the midchord-line sinks

C_{D_c} drag coefficient associated with the trailing-edge sources

C_{D_d} drag coefficient associated with the leading-edge image sinks

C_{D_e} drag coefficient associated with the midchord-line image
        sources

The derivation of the drag coefficients is performed for a wing of type 8, because the results for this wing type can be reduced to include every other wing type as a special case. No loss of generality is incurred by restricting the analysis to $M^2 = 2$ as will be subsequently explained.

The actual determinations of C_{D_a}, C_{D_b}, C_{D_c}, C_{D_d}, and C_{D_e} are carried out in Appendix A. The expressions for these drag coefficients are given in terms of τ, the tangent of the leading-edge

sweep angle, and $\frac{s}{c}$, the ratio of the semispan to the root chord. For a given value of aspect ratio and taper, the values of τ and $\frac{s}{c}$ are determined from the following expressions:

$$\tau = \frac{2(1-\lambda)}{A(1+\lambda)}$$

                                                                (4)

$$\frac{s}{c} = \frac{(1+\lambda)A}{4}$$

RESULTS AND DISCUSSION

Design Charts

Because the equations are too long to be very useful for direct computation of the drag coefficients, detailed calculations have been undertaken to determine drag charts based on these equations. Although the analysis and calculations have been performed for $M^2 = 2$, the drag charts have been generalized, as subsequently discussed, to be valid for all supersonic Mach numbers.

A given wing operating at $M^2 > 2$ or $M^2 < 2$ may be converted to an equivalent wing at $M^2 = 2$ by changing its lateral dimensions by the factor $\sqrt{M^2-1}$ and holding the thickness ratio constant. The effective aspect ratio of the equivalent wing is $A\sqrt{M^2-1}$, but its taper is the same as that of the given wing. During the lateral expansion or contraction the relative positions of the Mach lines and the wing are unchanged, and the pressure coefficients computed for the equivalent wing at $M^2=2$ will bear a point-to-point

correspondence with the pressure coefficients for the given wing at
$M^2 > 2$ or $M^2 < 2$. However, the pressure coefficients and the drag
coefficients for the equivalent wing must be divided by $\sqrt{M^2-1}$ to
convert them back to the given wing. From these considerations it
follows that plotting $C_D \sqrt{M^2-1}$ against $A\sqrt{M^2-1}$ for any taper
will give a chart which is applicable to all supersonic Mach numbers.

The drag coefficients, C_{D_a}, C_{D_b}, C_{D_c}, C_{D_d} and C_{D_e} have
all been calculated for $M^2 = 2$ and then have been added to give C_D,
the wing drag coefficient. Drag charts have then been constructed
to give $\dfrac{C_D}{\left(\frac{t}{c}\right)^2} \sqrt{M^2-1}$ as a function of $A\sqrt{M^2-1}$, the effective

aspect ratio, for various tapers. The drag chart for
$0 \leq A\sqrt{M^2-1} \leq 1.8$ is given in figure 4(a) and the drag chart for
$1.8 \leq A\sqrt{M^2-1} \leq 5.4$ is given in figure 4(b).

An examination of figure 4 reveals several points of interest.
For any Mach number greater than unity, the drag coefficient decreases
toward zero as the aspect ratio decreases toward zero. Also, as would
be expected the drag coefficients approach the section drag coeffi-
cient $\dfrac{4(t/c)^2}{\sqrt{M^2-1}}$ as the aspect ratio increases toward infinity. The
figure also shows that the effect of taper is generally greater at
small effective aspect ratios than at large effective aspect ratios.

Figure 4 also reveals the following information: The curves
of drag-coefficient parameter as a function of effective aspect
ratio are continuous for all tapers. However, all the curves have
discontinuities in slope except the curve for $\lambda = 1$. The
discontinuities in slope occur when the leading and trailing edges
are coincident with their Mach lines, and correspond to conditions
given by line III of figure 1. Slight decreases in effective aspect
ratios below those for this condition correspond to subsonic leading
and trailing edges and are accompanied by a rapid decrease in the
drag coefficient, particularly for small tapers. The wing having the
greatest drag coefficient is the wing of zero taper and effective
aspect ratio 2; that is, the wing with the leading edge parallel
to the Mach lines. This wing has a drag coefficient only about
15 percent greater than the section drag coefficient. Below an

effective aspect ratio of 1.75, wings of diamond plan form have the least drag; above this effective aspect ratio rectangular wings have the least drag.

As an example in the use of these charts to determine the wing drag coefficient, consider a wing of aspect ratio 2, taper 0.5, and of thickness 0.1 (same as semiwedge angle in radians for thin wings) flying at $M = 1.3$. Since $A\sqrt{M^2-1} = 1.662$, figure 4(a) gives

$$\frac{C_D}{\left(\frac{t}{c}\right)^2}\sqrt{M^2-1} = 4.23. \quad \text{Thus} \quad C_D = (0.1)^2 (1.204)(4.23) = 0.051.$$

It can be noted that the drag curve for the diamond plan-form wing may be used for wings incorporating a flat lower surface and an isosceles triangular section if the effective aspect ratio is greater than two. For such a wing with no tip and supersonic leading edges, the upper- and lower-surface pressures are independent so that the drag for the wing of isosceles triangular section is just half the drag for the wing of the same plan form, the section of which is a diamond formed by two of the isosceles triangles.

Magnitude of Individual Drag Coefficients for Wings

of Rectangular and Diamond Plan Form

The general formulas for the individual drag coefficients have been reduced to their particular forms for rectangular wings, and the results are given in Appendix B. The ratios of the individual drag coefficients to thickness ratio squared as functions of aspect ratio are given in figure 5(a) for $M^2=2$. The leading-edge sources produce uniform pressure over both front and rear surfaces and thus have no contribution to the drag. The ridge sinks account for a drag coefficient C_{D_b} equal to the section drag coefficient at all Mach numbers, which accounts for most of the wing drag.

From figure 5(a) it may also be seen that, above an aspect ratio of unity, C_{D_d} the drag associated with the leading-edge image sinks is just offset by C_{D_e} the thrust associated with the midchord-line image sources. Thus the tip does not affect the net wing drag although it does affect the spanwise distribution of the drag near the tips. Since the tip contributes no drag to the wing at aspect ratios greater than 1.0, the wing drag coefficient is independent of aspect ratios in this range and must be equal to the section drag coefficient.

For aspect ratios less than 1.0 the tip affects the wing drag in a manner such that the drag is reduced because the negative drag associated with the midchord-line image sources more than offsets the positive drag associated with the leading-edge image sinks. When the aspect ratio approaches zero, the thrust of the images is sufficient to overcome the drag associated with the midchord line, so that the drag coefficient also approaches zero.

Also in Appendix B the general formulas for the individual drag coefficients have been reduced to their particular form for wings of diamond plan form. These results have been used as the basis for figure 5(b) wherein the values of the ratio of the individual drag coefficients to the thickness ratio squared have been given as a function of aspect ratio for $M^2=2$.

With reference to figure 5(b), it can be seen that for aspect ratios greater than 2.0 the drag associated with the leading-edge sources is additive to that associated with the midchord line to make the wing drag coefficient greater than the section drag coefficient. For aspect ratios less than 2.0 the wing drag coefficient falls with decreasing aspect ratio as the result of several effects. First, the trailing edges of the wing are now subsonic and the positive pressures due to the trailing-edge sources extend onto the wing rear surfaces and act to decrease the drag. Second, the effect of the tip is to decrease the drag since the thrust associated with midchord image sources is greater than the drag associated with the leading-edge image sinks. Finally, the drag associated with the leading-edge sources decreases because the sweep of the sources increases as the aspect ratio becomes smaller.

The tip drag is represented by the difference between the drag associated with the leading-edge image sinks and the midchord-line image sources. For a rectangular wing with $A\sqrt{M^2-1}>1$ the drags identically cancel each other so that the tip drag is zero. This result is also true for other taper ratios as long as the Mach lines of the images intersect the trailing edge of their own half wing. It has also been found in other calculations not presented in this report that for tapered and untapered swept wings with a diamond profile and tips cut off in the stream direction the drag of the tip is zero, provided that the tip of one half wing does not affect the opposite half wing.

Variation of Drag Coefficient with Mach Number

Using the drag charts of figure 4, the variation with Mach number of $C_D/\left(\dfrac{t}{c}\right)^2$ has been determined for rectangular wings

of several aspect ratios and the results are presented in figure 6(a). The results show that for a given Mach number there exists a certain aspect ratio above which all rectangular wings have drag coefficients equal to the section drag coefficient. Thus all rectangular wings of aspect ratio greater than unity have the section drag coefficient at a Mach number greater than 1.41. At Mach numbers near unity very low-aspect-ratio wings show some reduction in drag compared with wings of higher aspect ratio.

The variation with Mach number $C_D/\left(\dfrac{t}{c}\right)^2$ has also been determined for wings of diamond plan form of several aspect ratios, and the results are presented in figure 6(b). The results show that considerable drag reduction is to be realized at Mach numbers near unity by reducing the aspect ratio.

CONCLUSIONS

The following conclusions may be drawn from the analysis within the limits of first-order theory; that is, insofar as the disturbance velocities are small and the effect of viscosity may be neglected.

1. Below an effective aspect ratio of 1.75, wings of diamond plan form have the least drag; above this effective aspect ratio rectangular wings have the least drag.

2. At very low effective aspect ratios, increasing the ratio of tip chord to root chord increases the drag coefficient markedly, but at large effective aspect ratios increasing the ratio of tip chord to root chord slightly decreases the drag coefficient.

3. Rectangular wings of effective aspect ratio greater than unity have a drag coefficient equal to the section drag coefficient.

4. For wings the tip Mach lines of which intersect the trailing edges on their own half wing, the tip effect does not change the net drag but changes only the distribution of the drag.

5. With decreasing effective aspect ratio for a given taper there is a sudden decrease in drag coefficient as the leading and trailing edges pass through the Mach cones.

6. At low effective aspect ratios the drag coefficient decreases with effective aspect ratio.

Ames Aeronautical Laboratory,
    National Advisory Committee For Aeronautics,
        Moffett Field, Calif.

APPENDIX A

DETERMINATION OF INDIVIDUAL DRAG COEFFICIENTS

Leading-edge Sources

Considering first the leading-edge sources, figure 3(a) shows the five areas of the half wing over which their pressure fields must be integrated to determine the drag coefficient C_{D_a}. Since there are two half wings and two sides to each half wing, and since the front surface is inclined at $+t/c$ radians to the flow and the rear surface is inclined at $-t/c$ radians to the flow

$$ S\ C_{D_a} = 4 \int_{S_1} P_a \left(\frac{t}{c}\right) dS_1 + 4 \int_{S_2} P_a \left(\frac{t}{c}\right) dS_2 + 4 \int_{S_3} P_a \left(\frac{t}{c}\right) dS_3 $$

$$ - 4 \int_{S_4} P_a \left(\frac{t}{c}\right) dS_4 - 4 \int_{S_5} P_a \left(\frac{t}{c}\right) dS_5 \tag{A1} $$

Considering both leading-edge sources, the pressure coefficient is given by equation (2) as follows:

$$ P_a = R.P. \frac{2t/c}{\pi \sqrt{\tau^2 - 1}} \left\{ \cosh^{-1} \left| \frac{\tau+\sigma}{1+\tau\sigma} \right| + \cosh^{-1} \left| \frac{\tau-\sigma}{1-\tau\sigma} \right| \right\} \tag{A2} $$

The differential areas taken as small triangles from the apex or as differences of the triangles are as follows:

$$ dS_1 = \frac{c^2}{8} d\sigma $$

$$ dS_2 = \frac{c^2}{8} d\sigma $$

$$ dS_3 = \frac{s^2}{2\sigma^2} d\sigma \tag{A3} $$

$$ dS_4 = \frac{s^2}{2\sigma^2} d\sigma - \frac{c^2}{8} d\sigma $$

$$ dS_5 = \frac{c^2}{2} \frac{d\sigma}{(1+\sigma\tau)^2} - \frac{c^2}{8} d\sigma $$

Substituting from equations (A2) and (A3) into equation (A1), putting in the limits shown in figure 3(a), and simplifying gives the following result:

$$S\ C_{D_a} = R.P.\ \frac{2\left(\dfrac{t}{c}\right)^2 c^2}{\pi\sqrt{\tau^2-1}}\left\{\int_0^{\frac{2s}{c}}\left[\cosh^{-1}\left|\frac{\tau+\sigma}{1+\tau\sigma}\right| + \cosh^{-1}\left|\frac{\tau-\sigma}{1-\tau\sigma}\right|\ \right]d\sigma\right.$$

$$+\ 2\frac{s^2}{c^2}\int_{\frac{2s}{c}}^{\frac{1}{\tau}}\left[\cosh^{-1}\left|\frac{\tau+\sigma}{1+\tau\sigma}\right| + \cosh^{-1}\left|\frac{\tau-\sigma}{1-\tau\sigma}\right|\ \right]\frac{d\sigma}{\sigma^2}$$

$$-\ 2\frac{s^2}{c^2}\int_{\frac{s}{c-s\tau}}^{\frac{2s}{c}}\left[\cosh^{-1}\left|\frac{\tau+\sigma}{1+\tau\sigma}\right| + \cosh^{-1}\left|\frac{\tau-\sigma}{1-\tau\sigma}\right|\ \right]\frac{d\sigma}{\sigma^2}$$

$$\left.-\ 2\int_0^{\frac{s}{c-s\tau}}\left[\cosh^{-1}\left|\frac{\tau+\sigma}{1+\tau\sigma}\right| + \cosh^{-1}\left|\frac{\tau-\sigma}{1-\tau\sigma}\right|\ \right]\frac{d\sigma}{(1+\tau\sigma)^2}\right\}\qquad(A4)$$

Carrying out the integration, collecting similar terms, and making the following substitution for the wing area $S = 2\ sc\ (1-s\ \tau/c)$ gives the drag coefficient.

$$C_{D_a} = \text{R.P.} \frac{\left(\frac{t}{c}\right)^2 \left(\frac{c}{s}\right)}{\pi \sqrt{\tau^2-1}(1-s\tau/c)} \left\{ \frac{2\sqrt{\tau^2-1}}{\tau} \sin^{-1}(2s/c) \right.$$

$$+ \frac{(1+2s\tau/c)^2}{\tau} \cosh^{-1}\left[\frac{\tau+2s/c}{1+2s\tau/c}\right] - \frac{(1-2s\tau/c)^2}{\tau} \cosh^{-1}\left[\frac{\tau-2s/c}{1-2s\tau/c}\right]$$

$$+ \frac{(1-3\tau^2)+4(\tau^2-1)s\tau/c}{\tau(1-\tau^2)} \cosh^{-1}[\tau-s(\tau^2-1)/c]$$

$$+ \frac{(1-2s\tau/c)^2}{\tau} \cosh^{-1}\left[\frac{\tau-s(\tau^2+1)/c}{1-2s\tau/c}\right] - \frac{2(2\tau^2-1)}{\tau(\tau^2-1)} \cosh^{-1}\tau$$

$$+ \frac{2}{\sqrt{\tau^2-1}} - \frac{2\sqrt{(1-s\tau/c)^2-(s/c)^2}}{\sqrt{\tau^2-1}} - \frac{4s^2\tau}{c^2} \cosh^{-1}\left(\frac{\tau+1}{2\tau}\right) \right\} \qquad (A5)$$

Midchord-line Sinks

A simple expression can be derived for the drag coefficient associated with the pair of sinks along the midchord line. From equation (1) the pressure drop for the flow deflected through an angle $-2\left(\frac{t}{c}\right)$ by the sinks is

$$P_b = - \frac{4\left(\frac{t}{c}\right)}{\pi} \left[\cos^{-1}(-\sigma) + \cos^{-1}(\sigma)\right] = - 4\left(\frac{t}{c}\right) \qquad (A6)$$

Since the pressure coefficient acts uniformly over the upper and lower rear surfaces to cause drag,

$$C_{D_b} = 4\left(\frac{t}{c}\right)^2 \qquad (A7)$$

Trailing-edge Sources

The sources along the trailing edges (fig. 3(d)) act always
to decrease the drag as their positive pressure field may act only
on the rear surface of the wing. The drag coefficient is given by
the following equation:

$$S \, C_{D_c} = -4 \int_{S_1} P_c \left(\frac{t}{c}\right) dS_1 \qquad (A8)$$

The pressure coefficient for one source from equation (2) is

$$P_c = \text{R.P.} \, \frac{2t/c}{\pi \sqrt{\tau^2 - 1}} \cosh^{-1} \left|\frac{\tau - \sigma}{1 - \tau\sigma}\right| \qquad (A9)$$

and the differential area is

$$dS = 2s^2 \tau^2 \frac{d\sigma}{(1+\tau\sigma)^2} \qquad (A10)$$

Substituting from equations (A9) and (A10) into equation (A8),
carrying out the integration, and simplifying gives the drag coeffi-
cient

$$C_{D_c} = -\text{R.P.} \, \frac{4 \left(\frac{t}{c}\right)^2 \left(\frac{s}{c}\right) \tau}{\pi \sqrt{\tau^2 - 1} \, (1 - s\tau/c)} \cosh^{-1} \left|\frac{\tau^2 + 1}{2\tau}\right|$$

Leading-edge Image Sinks

The image sinks associated with the leading-edge sources produce
pressures on the wing which tend to increase the wing drag. Referring
to figure 3(b), the drag coefficient can be written as follows:

$$S \, C_{D_d} = 4 \int_{S_1} P_d \left(\frac{t}{c}\right) dS_1 - 4 \int_{S_2} P_d \left(\frac{t}{c}\right) dS_2 - 4 \int_{S_3} P_d \left(\frac{t}{c}\right) dS_3$$

$$- 4 \int_{S_4} P_d \left(\frac{t}{c}\right) dS_4 + 4 \int_{S_5} P_d \left(\frac{t}{c}\right) dS_5 \qquad (A11)$$

The differential areas are given by the following equations:

$$dS_1 = \frac{\lambda^2 c^2}{8} \, d\sigma$$

$$dS_2 = \frac{\lambda^2 c^2}{2} \frac{d\sigma}{(1-\tau\sigma)^2} - \frac{\lambda^2 c^2}{8} \, d\sigma$$

$$dS_3 = \frac{c^2}{2} \frac{d\sigma}{(1+\tau\sigma)^2} - \frac{\lambda^2 c^2}{8} \, d\sigma \qquad (A12)$$

$$dS_4 = 2s^2 \frac{d\sigma}{\sigma^2} - \frac{\lambda^2 c^2}{8} \, d\sigma$$

$$dS_5 = 2s^2 \frac{d\sigma}{\sigma^2}$$

The pressure coefficient can be obtained by an application of equation (2).

$$P_d = - \text{R.P.} \, \frac{2 \, t/c}{\pi \sqrt{\tau^2-1}} \cosh^{-1} \left| \frac{\tau+\sigma}{1+\tau\sigma} \right| \qquad (A13)$$

Substituting from equations (A12) and (A13) back into equation (A11), putting in the limits shown in figure 3(b), and simplifying gives the drag coefficient.

$$S \, C_{D_d} = \text{R.P.} \, \frac{2 \left(\frac{t}{c}\right)^2 c^2}{\pi\sqrt{\tau^2-1}} \left[-\lambda^2 \int_0^{\frac{4s}{c-2s\tau}} \cosh^{-1} \left| \frac{\tau+\sigma}{1+\tau\sigma} \right| d\sigma \right.$$

$$+ 2\lambda^2 \int_0^{\frac{s}{c-s\tau}} \cosh^{-1} \left| \frac{\tau+\sigma}{1+\tau\sigma} \right| \frac{d\sigma}{(1-\tau\sigma)^2} + 2 \int_{\frac{s}{c-s\tau}}^{\frac{2s}{c-2s\tau}} \cosh^{-1} \left| \frac{\tau+\sigma}{1+\tau\sigma} \right| \frac{d\sigma}{(1+\tau\sigma)^2}$$

$$+ \frac{8s^2}{c^2} \int_{\frac{2s}{c-2s\tau}}^{\frac{4s}{c-2s\tau}} \cosh^{-1} \left| \frac{\tau+\sigma}{1+\tau\sigma} \right| \frac{d\sigma}{\sigma^2} - \frac{8s^2}{c^2} \int_{\frac{4s}{c-2s\tau}}^{1} \cosh^{-1} \left(\frac{\tau+\sigma}{1+\tau\sigma} \right) \frac{d\sigma}{\sigma^2} \right]$$

$$(A14)$$

Carrying out the integration, collecting similar terms, and substituting $S = 2sc(1-s\tau/c)$ gives the drag coefficient.

$$C_{D_d} = \text{R.P.} \frac{\left(\frac{t}{c}\right)^2 \left(\frac{c}{s}\right)}{\pi\sqrt{\tau^2-1}(1-s\tau/c)} \left\{ -\frac{(1+2s\tau/c)^2}{\tau}\cosh^{-1}\left[\frac{\tau-2s(\tau^2-2)/c}{1+2s\tau/c}\right] \right.$$

$$-\frac{(1-2s\tau/c)^2}{\tau}\sqrt{\tau^2-1}\sin^{-1}\frac{4s/c}{1-2s\tau/c} - \frac{(1-2s\tau/c)^2}{\tau}\cosh^{-1}\tau$$

$$+\frac{[(3\tau^2-1)+4s\tau(1-\tau^2)/c]}{\tau(\tau^2-1)}\cosh^{-1}[\tau-s(\tau^2-1)/c]$$

$$+\frac{(1-2s\tau/c)^2}{\tau}\cosh^{-1}\left[\frac{\tau-s(\tau^2+1)/c}{1-2s\tau/c}\right]$$

$$-\frac{2[\tau-4s(\tau^2-1)/c]}{(\tau^2-1)}\cosh^{-1}[\tau-2s(\tau^2-1)/c] + 2\frac{\sqrt{(1-2s\tau/c)^2-(2s/c)^2}}{\sqrt{\tau^2-1}}$$

$$-\frac{2\sqrt{(1-s\tau/c)^2-(s/c)^2}}{\sqrt{\tau^2-1}} + \frac{16s^2}{c^2}\sqrt{\tau^2-1}\cosh^{-1}\left(\frac{1-2s\tau/c}{4s/c}\right)$$

$$\left. -\frac{8s^2}{c^2}\sqrt{\tau^2-1}\cosh^{-1}\left(\frac{1-2s\tau/c}{2s/c}\right) \right\} \tag{A15}$$

Midchord-line Image Sources

The image sources associated with the midchord-line produce positive pressures on the rear surfaces of the wing and tend to reduce the drag. Referring to figure 3(c), the drag coefficient can be written as follows:

$$S \ C_{D_e} = - 4 \int_{S_1} P_e \left(\frac{t}{c}\right) dS_1 - 4 \int_{S_2} P_e \left(\frac{t}{c}\right) dS_2 - 4 \int_{S_3} P_e \left(\frac{t}{c}\right) dS_3 \quad (A16)$$

The differential areas can be written as follows:

$$dS_1 = \frac{\lambda^2 c^2}{8} \frac{d\sigma}{(1-\tau\sigma)^2}$$

$$dS_2 = \frac{c^2}{8} (1+2s\tau/c)^2 \frac{d\sigma}{(1+\tau\sigma)^2} \qquad (A17)$$

$$dS_3 = 2s^2 \frac{d\sigma}{\sigma^2}$$

The pressure coefficient may be obtained by an application of equation (1).

$$P_e = \frac{4t/c}{\pi} \cos^{-1}(\sigma) \qquad (A18)$$

Substituting from equations (A17) and (A18) into equation (A16), putting in the limits shown in figure 3(c), and simplifying gives the drag coefficient.

$$S \ C_{D_e} = - \text{R.P.} \ \frac{2\left(\frac{t}{c}\right)^2 c^2}{\pi} \left[\lambda^2 \int_0^{\frac{2s}{c}} \cos^{-1}(\sigma) \frac{d\sigma}{(1-\tau\sigma)^2} \right.$$

$$\left. + (1+2s\tau/c)^2 \int_{\frac{2s}{c}}^{\frac{4s}{c-2s\tau}} \cos^{-1}(\sigma) \frac{d\sigma}{(1+\tau\sigma)^2} + \frac{16s^2}{c^2} \int_{\frac{4s}{c-2s\tau}}^1 \cos^{-1}(\sigma) \frac{d\sigma}{\sigma^2} \right]$$

$$(A19)$$

Carrying out the integration, collecting similar terms, and making the substitution, $S = 2sc(1-s\tau/c)$, gives the drag coefficient.

$$C_{D_e} = - \text{R.P.} \frac{\left(\frac{t}{c}\right)^2 \left(\frac{c}{s}\right)}{\pi(1-s\tau/c)} \left\{ \frac{2}{\tau} \cos^{-1}(2s/c) \right.$$

$$- \frac{\pi(1-2s\tau/c)^2}{2\tau} + \frac{(1-2s\tau/c)^2}{\tau\sqrt{\tau^2-1}} \cosh^{-1}\left[\frac{\tau-2s/c}{1-2s\tau/c}\right]$$

$$- \frac{(1-2s\tau/c)^2}{\tau\sqrt{\tau^2-1}} \cosh^{-1}\tau - \frac{(1-2s\tau/c)^2}{\tau} \cos^{-1}\left[\frac{4s/c}{1-2s\tau/c}\right]$$

$$+ \frac{(1+2s\tau/c)^2}{\tau\sqrt{\tau^2-1}} \cosh^{-1}\left[\frac{\tau-2s(\tau^2-2)/c}{1+2s\tau/c}\right]$$

$$- \frac{(1+2s\tau/c)^2}{\tau\sqrt{\tau^2-1}} \cosh^{-1}\left(\frac{\tau+2s/c}{1+2s\tau/c}\right) - \frac{16s^2}{c^2} \cosh^{-1}\left[\frac{1-2s\tau/c}{4s/c}\right] \left. \right\} \qquad (A20)$$

APPENDIX B

REDUCTION OF GENERAL EQUATIONS FOR WINGS OF
RECTANGULAR AND DIAMOND PLAN FORM

The general formulas for the individual drag coefficient can be
considerably simplified for wings of rectangular or diamond plan form.
For the rectangular plan form the formulas are simplified by determin-
ing the limiting values of the drag coefficients as τ, the tangent
of the leading-edge sweepback angle, approaches zero since the formulas
are indeterminate for $\tau = 0$. The actual limiting process is lengthy
and only the results are given here.

$$C_{D_a} = 0$$

$$C_{D_b} = 4 \left(\frac{t}{c}\right)^2$$

$$C_{D_c} = 0$$

$$C_{D_d} = \text{R.P.} \ \frac{\left(\frac{t}{c}\right)^2 \left(\frac{c}{s}\right)}{\pi} \left[8 \ \frac{s}{c} \ \cos^{-1} \ \frac{2s}{c} \ - \ 2\sqrt{1-(2s/c)^2} \ + \ 1 \right.$$

$$\left. - \ \frac{8s^2}{c^2} \ \cosh^{-1}\left(\frac{c}{2s}\right) \ + \ \sqrt{1-(4s/c)^2} \ + \ \frac{16s^2}{c^2} \ \cosh^{-1}\left(\frac{c}{4s}\right) - \ \frac{8s}{c} \ \cos^{-1}\left(\frac{4s}{c}\right) \right]$$

$$\text{(B1)}$$

$$C_{D_e} = \text{R.P.} \ - \ \frac{\left(\frac{t}{c}\right)^2 \left(\frac{c}{s}\right)}{\pi} \left[1 \ + \ \frac{8s}{c} \ \cos^{-1}\left(\frac{4s}{c}\right) - \sqrt{1-(4s/c)^2} \ - \ \frac{16s^2}{c^2} \ \cosh^{-1}\left(\frac{c}{4s}\right) \right]$$

Summing the component drag coefficients and making the substitution
$A = 2s/c$ gives the wing drag coefficient in terms of the aspect ratio.

$$C_D = R.P. \ 4 \left(\frac{t}{c}\right)^2 \left[1 - \frac{1}{\pi} \left(\frac{\sqrt{1-A^2}}{A} + A \ \cosh^{-1} \frac{1}{A} - 2 \ \cos^{-1} A \right) \right.$$

$$\left. - \frac{1}{\pi} \left(- \frac{\sqrt{1-4A^2}}{A} - 4A \ \cosh^{-1} \frac{1}{2A} + 4 \ \cos^{-1} 2A \right) \right] \quad (B2)$$

Inspection of equation (B2) shows that the first term is real for all aspect ratios, that the next three terms are real only for aspect ratios less than unity, and that the last three terms are real only for aspect ratios less than one-half.

In simplifying the general formulas for wings of diamond plan form it is sufficient to substitute the condition for zero taper $\tau = c/2s$, since the formulas are determinate for this case. The following results have been obtained.

$$C_{D_a} = R.P. \frac{4 \left(\frac{t}{c}\right)^2 \tau}{\pi \sqrt{\tau^2-1}} \left\{ \frac{2(2\tau^2-1)}{\tau(1-\tau^2)} \left[\cosh^{-1} \tau - \cosh^{-1} \left(\frac{\tau^2+1}{2\tau} \right) \right] \right.$$

$$\left. + \frac{2}{\tau} \sqrt{\tau^2-1} \ \sin^{-1} \left(\frac{1}{\tau}\right) + \frac{2}{\sqrt{\tau^2-1}} - \frac{1}{\tau} \right\}$$

$$C_{D_b} = 4 \left(\frac{t}{c}\right)^2 \qquad\qquad\qquad\qquad\qquad\qquad\qquad\qquad\qquad (B3)$$

$$C_{D_c} = R.P. \frac{-4 \left(\frac{t}{c}\right)^2}{\pi \sqrt{\tau^2-1}} \ \cosh^{-1} \left(\frac{\tau^2+1}{2\tau} \right)$$

$$C_{D_d} = R.P. \frac{4 \left(\frac{t}{c}\right)^2}{\pi \sqrt{\tau^2-1}} \left\{ \frac{\tau^2+1}{\tau^2-1} \ \cosh^{-1} \left(\frac{\tau^2+1}{2\tau} \right) - 1 \right\}$$

$$C_{D_e} = R.P. \frac{-8 \left(\frac{t}{c}\right)^2}{\pi} \left\{ \cos^{-1} \left(\frac{1}{\tau}\right) - \frac{2}{\sqrt{\tau^2-1}} \cosh^{-1} \left(\frac{\tau^2+1}{2\tau} \right) \right\}$$

Summing the component drag coefficients and making the substitution $A = 2/\tau$ gives the following formula for the drag coefficient of a diamond plan-form wing:

$$C_D = R.P. \frac{8 \left(\frac{t}{c}\right)^2 A}{\pi \sqrt{4-A^2}} \left\{ \frac{2}{\sqrt{4-A^2}} - 1 + \frac{A}{2} \sqrt{4-A^2} \sin^{-1}\left(\frac{A}{2}\right) \right.$$

$$\left. + \left(\frac{8-A^2}{4-A^2}\right) \left[2 \cosh^{-1}\left(\frac{4+A^2}{4A}\right) - \cosh^{-1}\left(\frac{2}{A}\right) \right] \right\} \tag{B4}$$

When the leading edges of the wing are swept behind the Mach cone, $\tau > 1$ and $A < 2$ so that all terms of equations (B3) and (B4) are real. However, for leading edges in front of the Mach cone where $\tau < 1$ and $A > 2$, use must be made of the following relationship to find the real part of equations (B3) and (B4):

$$\frac{\cos^{-1} x}{\sqrt{1-\tau^2}} = \frac{\cosh^{-1} x}{\sqrt{\tau^2-1}} \tag{B5}$$

The resulting equations for the component drag coefficients and wing drag coefficient are as follows:

$$C_{D_a} = \frac{4\tau\left(\frac{t}{c}\right)^2}{\pi\sqrt{1-\tau^2}} \left[\frac{\pi\sqrt{1-\tau^2}}{\tau} - \frac{2}{\sqrt{1-\tau^2}} - \frac{2(1-2\tau^2)}{\tau(1-\tau^2)} \cos^{-1} \tau \right]$$

$$C_{D_b} = 4\left(\frac{t}{c}\right)^2 \qquad\qquad\qquad\qquad\qquad\qquad\qquad\qquad\qquad (B6)$$

$$C_{D_c} = C_{D_d} = C_{D_e} = 0$$

$$C_D = \frac{16 \left(\frac{t}{c}\right)^2}{\pi \sqrt{A^2-4}} \left[\frac{\pi}{2} \sqrt{A^2-4} - \frac{A}{\sqrt{A^2-4}} - \frac{A(A^2-8)}{2(A^2-4)}\cos^{-1}\left(\frac{2}{A}\right) \right] \tag{B7}$$

REFERENCES

1. Jones, Robert T.: Thin Oblique Airfoils at Supersonic Speed.
       NACA TN No. 1107, 1946.

2. Puckett, Allen E.: Supersonic Wave Drag of Thin Airfoils
       Jour. Aero. Sci., vol. 13, no. 9, Sept. 1946, pp. 475–484.

3. Harmon, Sidney M., and Swanson, Margaret D.: Calculations of
       the Supersonic Wave Drag of Nonlifting Wings with Arbitrary
       Sweepback and Aspect Ratio. Wings Swept Behind the Mach Lines.
       NACA TN No. 1319, 1947.

4. Taylor, G.I.: Applications to Aeronautics of Ackeret's Theory
       of Aerofoils Moving at Speeds Greater than that of Sound.
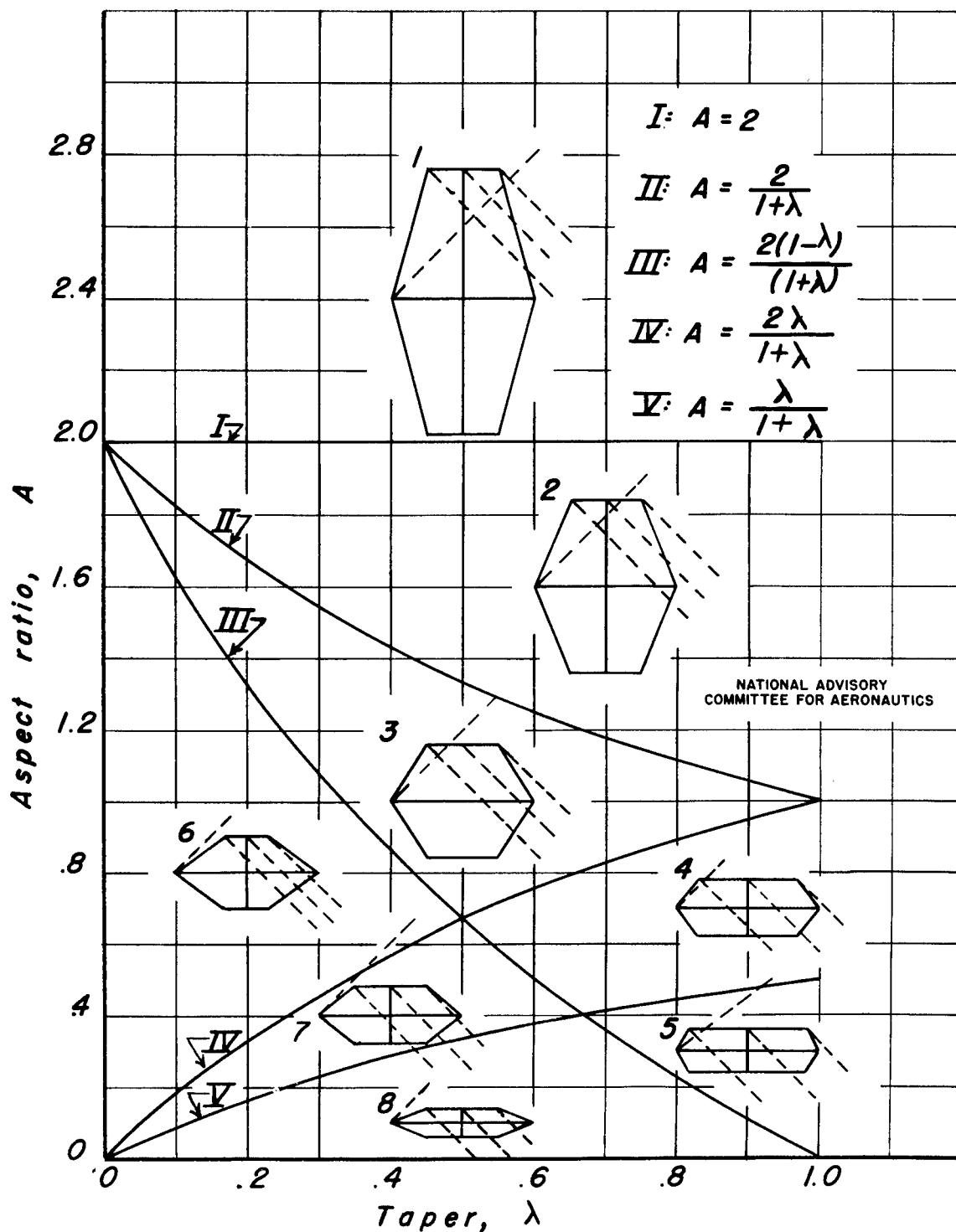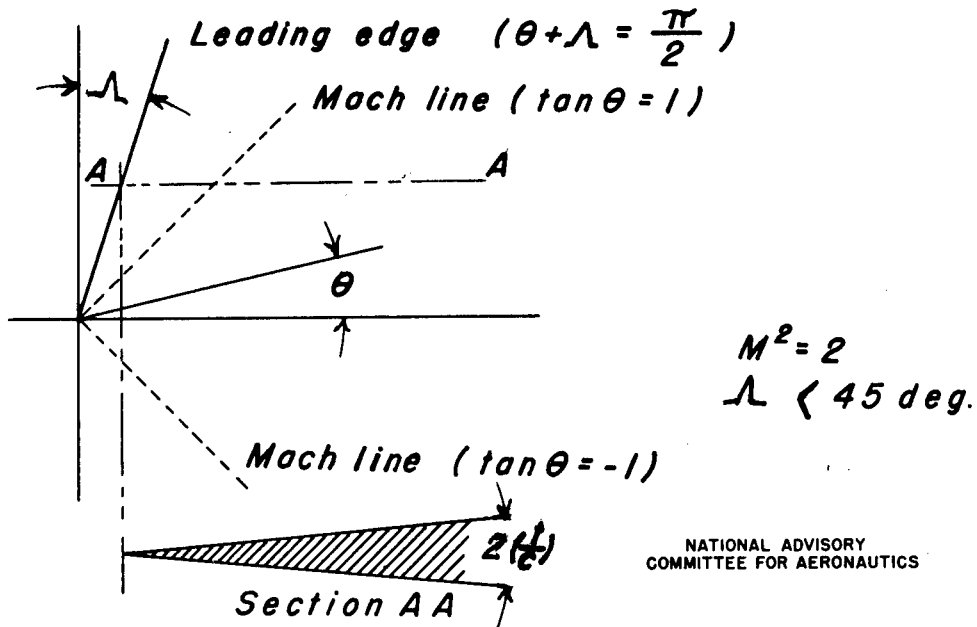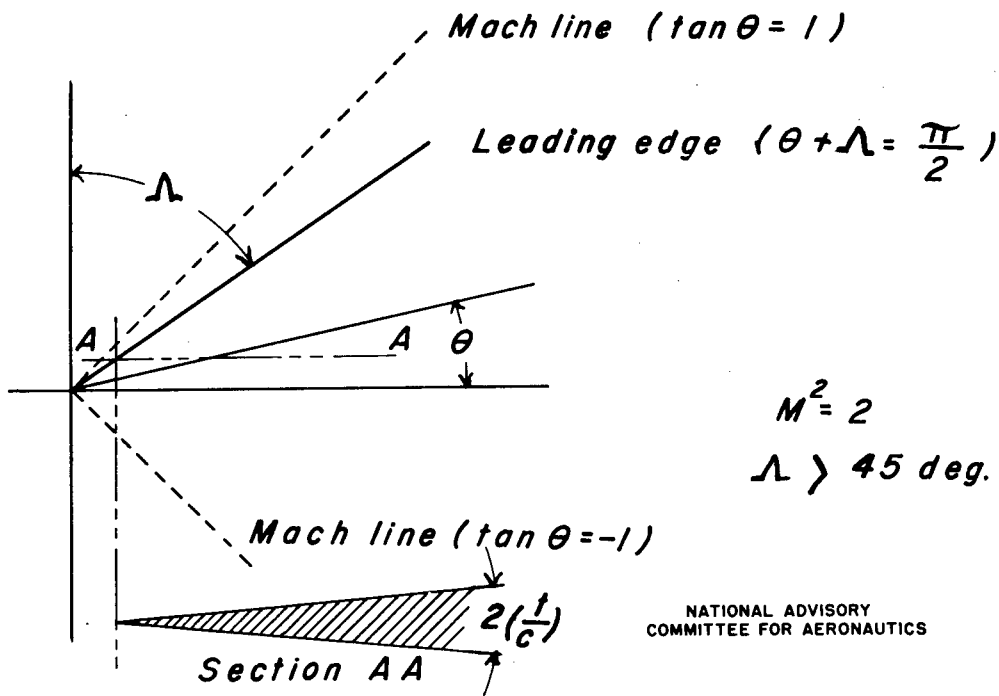   R.& M. No. 1467, British A.R.C., 1932.

$$I: \quad A = 2$$

$$II: \quad A = \frac{2}{1+\lambda}$$

$$III: \quad A = \frac{2(1-\lambda)}{(1+\lambda)}$$

$$IV: \quad A = \frac{2\lambda}{1+\lambda}$$

$$V: \quad A = \frac{\lambda}{1+\lambda}$$

NATIONAL ADVISORY
COMMITTEE FOR AERONAUTICS

Figure 1.- Subdivision of wings into
eight types for $M^2 = 2$

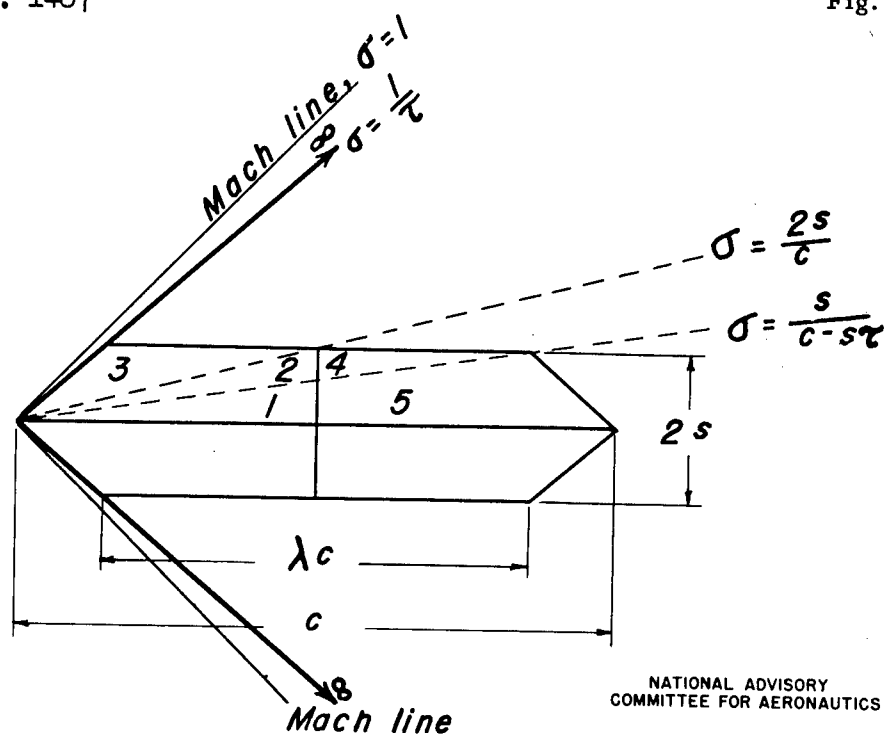Fig. 2 a, b   NACA TN No. 1487

Leading edge $(\theta + \Lambda = \frac{\pi}{2})$

Mach line $(\tan \theta = 1)$

A ----------------- A

θ

$M^2 = 2$

$\Lambda < 45 \deg.$

Mach line $(\tan \theta = -1)$

$2(\frac{t}{c})$

Section A A

(a)   Supersonic leading edge

Mach line $(\tan \theta = 1)$

Leading edge $(\theta + \Lambda = \frac{\pi}{2})$

A A θ

$M^2 = 2$

$\Lambda > 45 \deg.$

Mach line $(\tan \theta = -1)$

$2(\frac{t}{c})$

Section A A

(b) Subsonic leading edge

**Figure 2.- Symmetrical semi-infinite wedges of
Jones' basic solution**
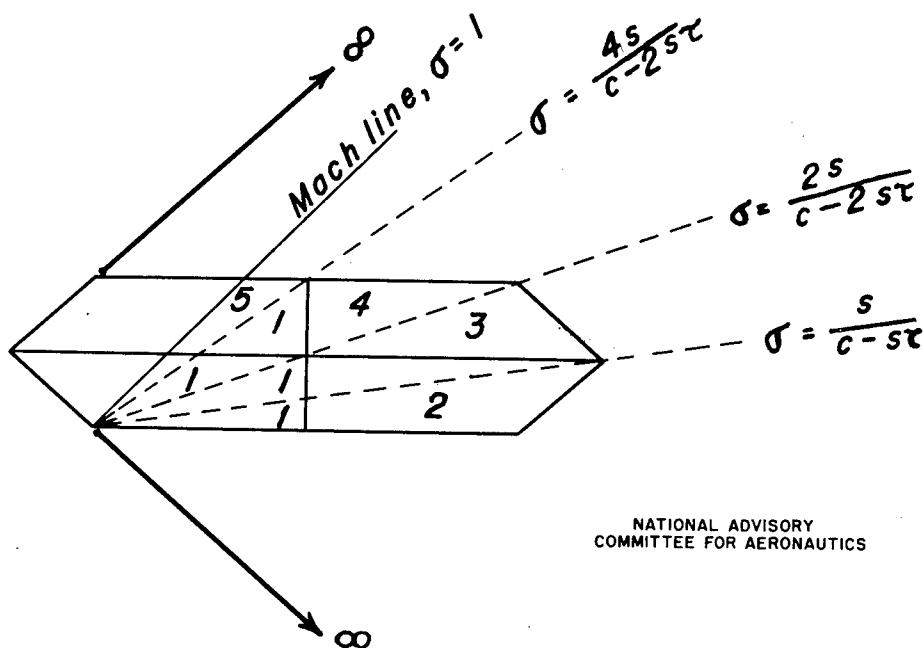
(a) Leading-edge sources
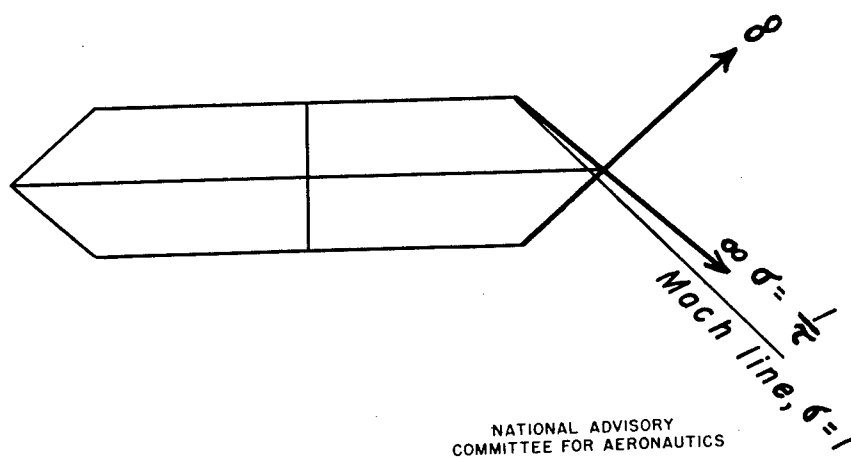

(b) Leading-edge image sinks

Figure 3.- Sources, sinks, integration areas, and limits
for determining wing drag coefficient

Fig. 3 c, d

NACA TN No. 1487

Mach line, $\sigma = 1$

$\sigma = \dfrac{4s}{c - 2s\tau}$

$\sigma = \dfrac{2s}{c}$

3 2
3 2 1

NATIONAL ADVISORY
COMMITTEE FOR AERONAUTICS
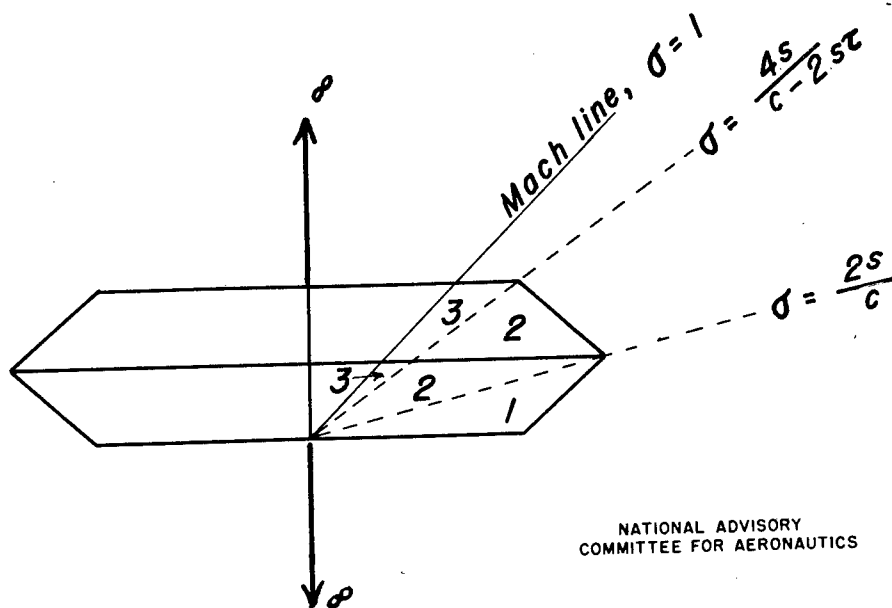
(c) Midchord-line image sources

∞ $\sigma = \dfrac{1}{\tau}$
Mach line, $\sigma = 1$

NATIONAL ADVISORY
COMMITTEE FOR AERONAUTICS

(d) Trailing-edge sources

Figure 3— Concluded

Fig. 4 a

Effective aspect ratio, $A \sqrt{M^2 - 1}$

(a) Low aspect ratio range

Drag coefficient parameter, $\dfrac{C_D \sqrt{M^2 - 1}}{\left(\frac{t}{c}\right)^2}$
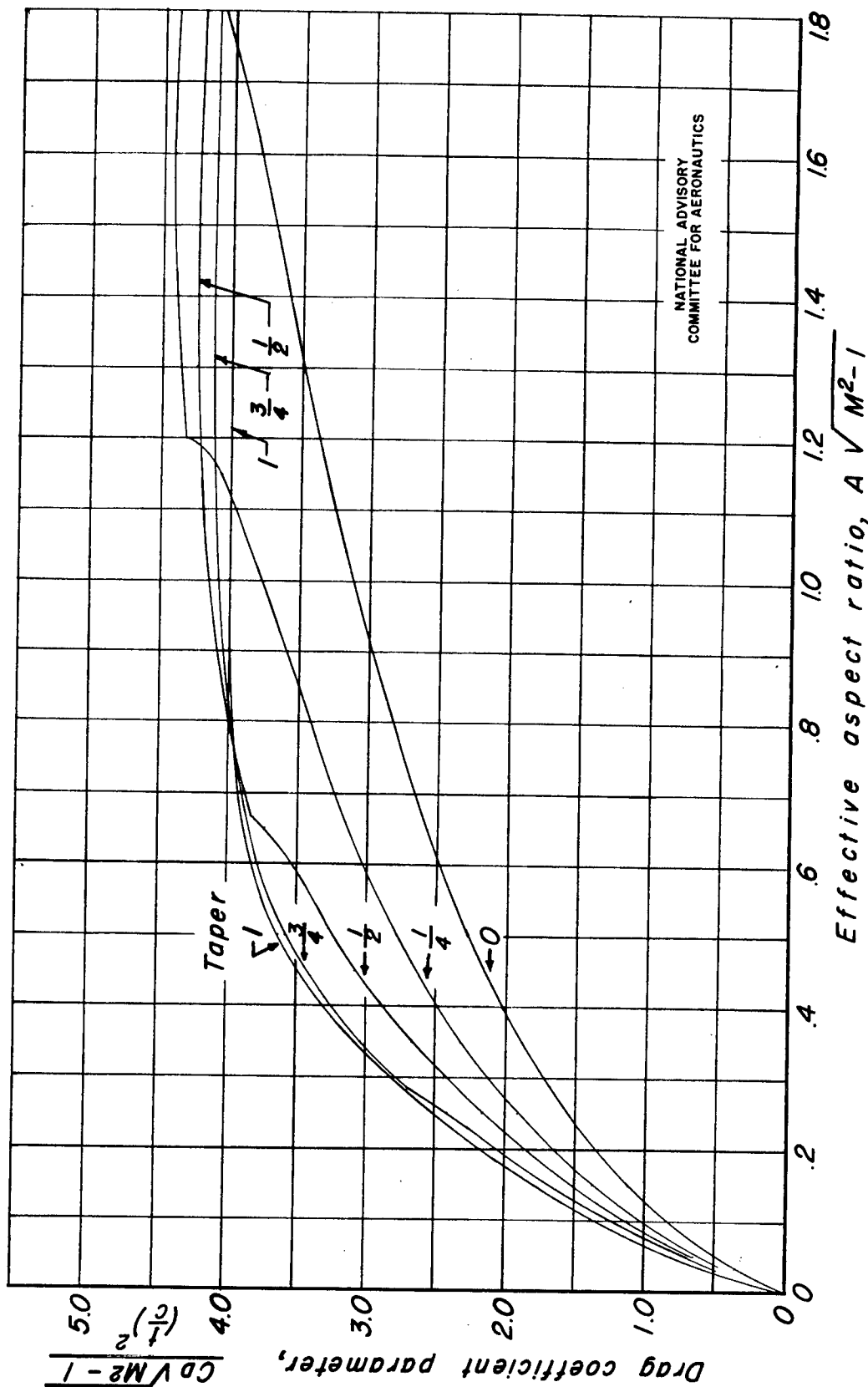
Figure 4.- Chart for determining pressure drag coefficient at zero lift, diamond airfoil section

NATIONAL ADVISORY
COMMITTEE FOR AERONAUTICS

Fig. 4 b

NACA TN No. 1487

Effective aspect ratio, $A\sqrt{M^2-1}$

Drag coefficient parameter, $\dfrac{C_D\sqrt{M^2-1}}{\left(\dfrac{t}{c}\right)^2}$

Taper
0

$\dfrac{1}{4}$

$\dfrac{1}{2}$

$\dfrac{3}{4}$

1

NATIONAL ADVISORY
COMMITTEE FOR AERONAUTICS
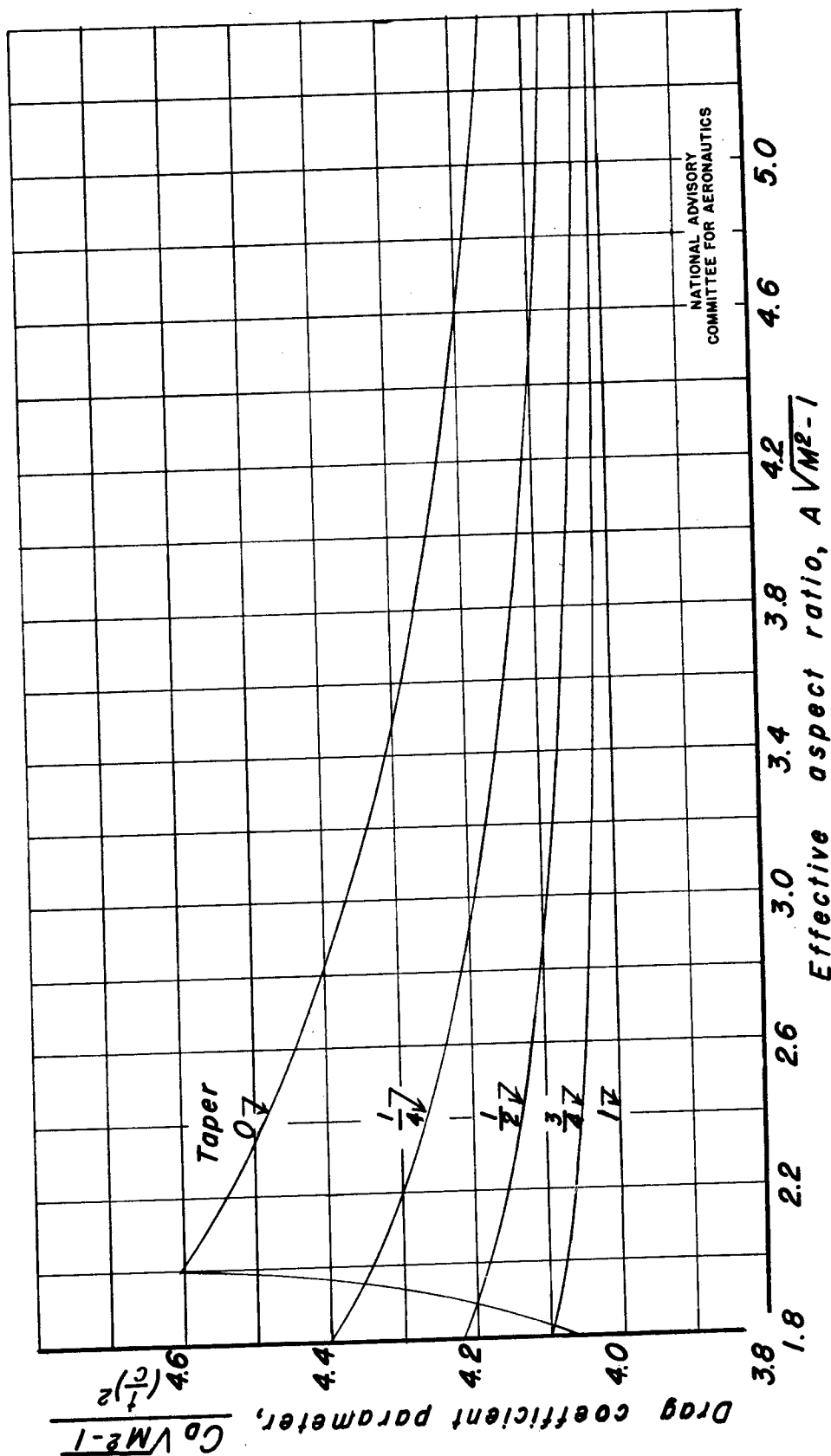
(b) High aspect ratio range
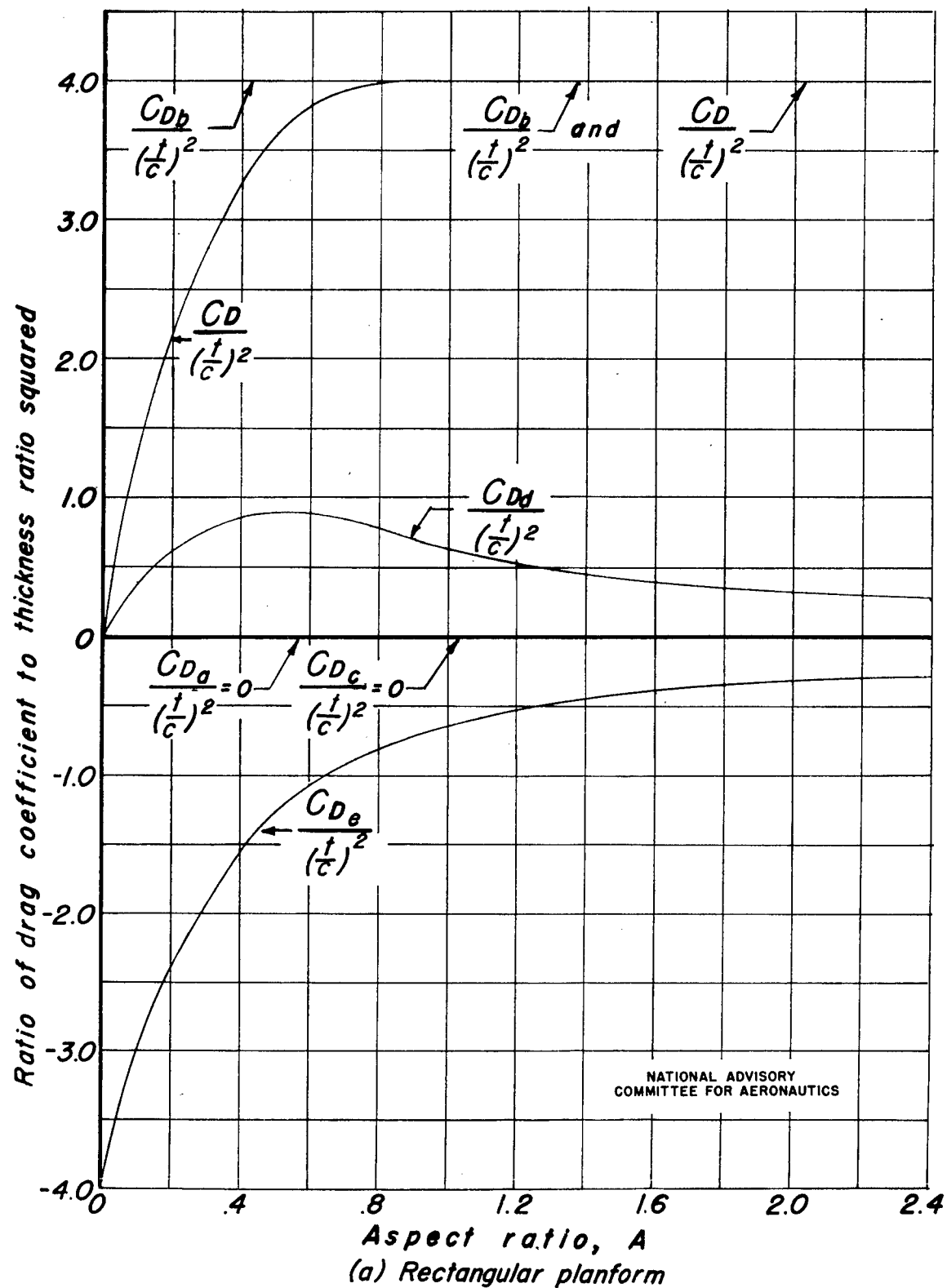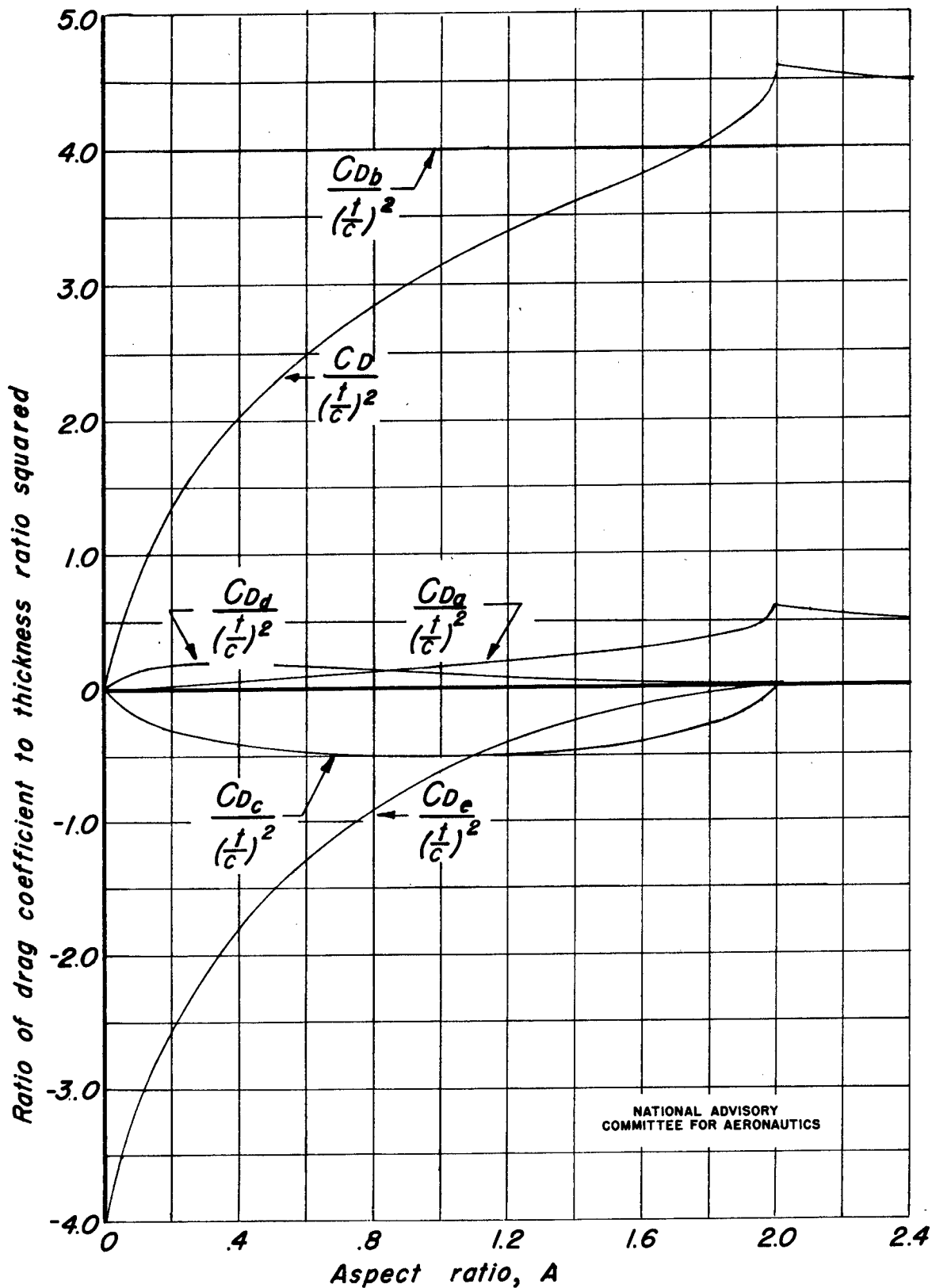
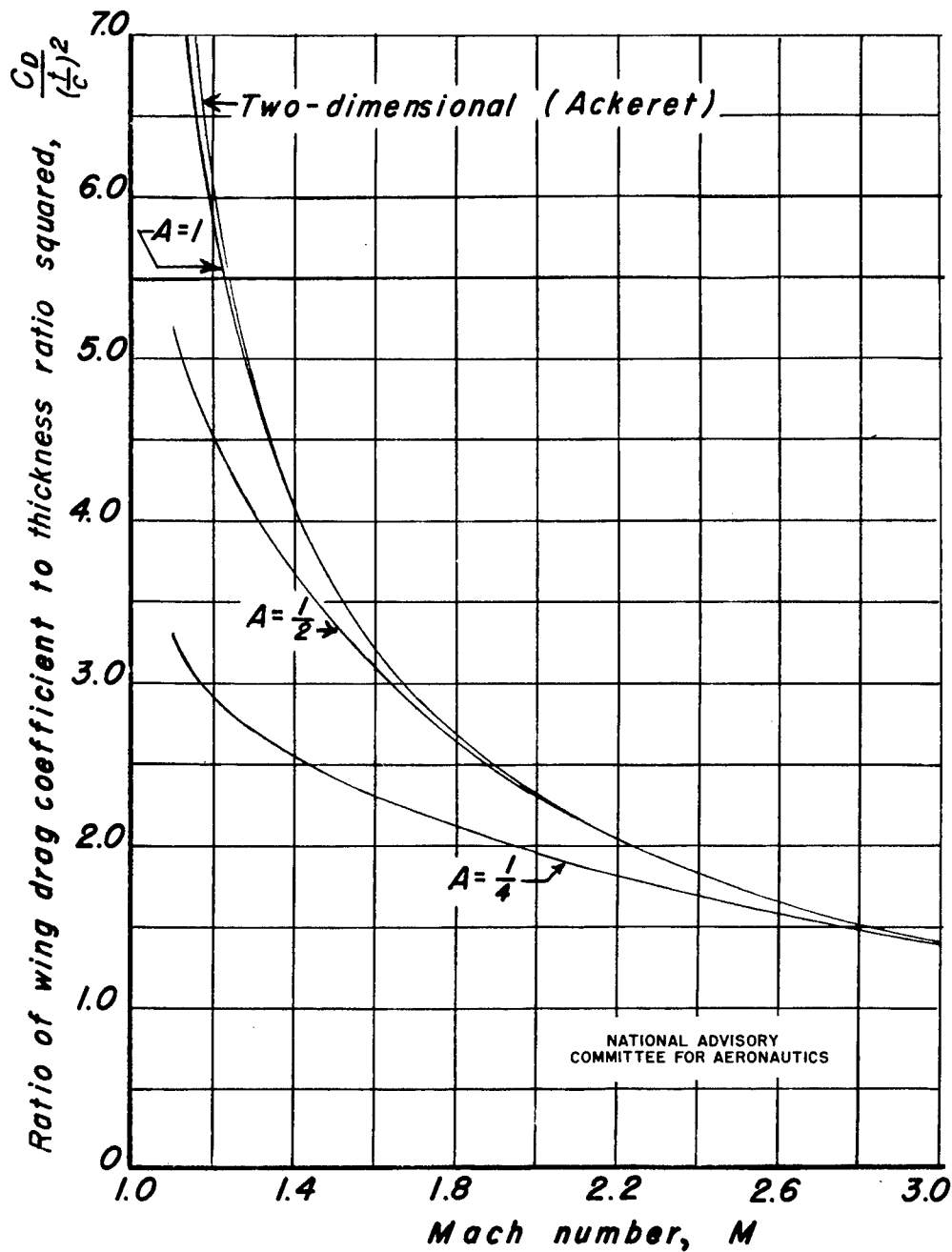Figure 4.- Concluded

Fig. 5 a

(a) Rectangular planform

Figure 5.— Ratio of individual drag coefficients to thickness ratio squared as a function of aspect ratio at $M^2 = 2$
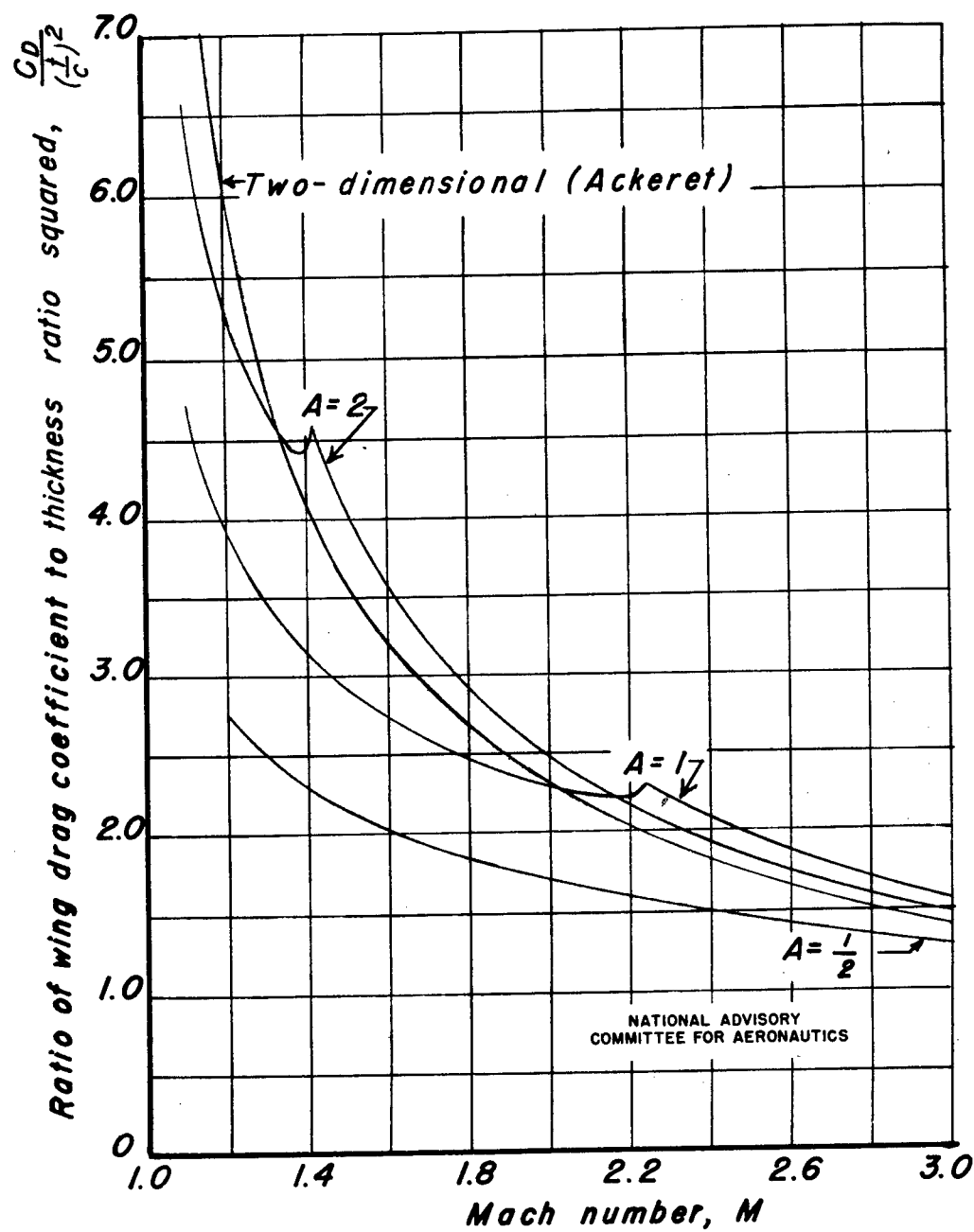
Fig. 5 b

NACA TN No. 1487

Aspect ratio, A

(b) Diamond planform

Figure 5.– Concluded

(a) Rectangular planform

Figure 6.— Ratio of wing drag coefficients to thickness
ratio squared for several aspect ratios   as a function
of Mach number

Fig. 6 b

NACA TN No. 1487

(b) Diamond planform
Figure 6.- Concluded